CONSTITUIVE MODELLING OF CLAYS AND SANDS USING THE CRITICAL STATE FRAMEWORK

Elliot James Fern & Kenichi Soga

Department of Engineering

University of Cambridge

1. INTRODUCTION

The aim of this chapter is to present the stress-strain relationships of clay and sand through their constitutive models developed from the critical state theory. Two families of models are presented (Cam-Clay and Nor-Sand), explained and illustrated. These critical state based models provide a powerful mathematical tool for engineering practice.

The critical state theory **(Roscoe et al. 1958)** and its associated framework **(Schofield and Wroth 1968)**, described in the **Chapter 1**, will be used as a reference theory for the development of constitutive models for clays and sands. The critical state theory was developed for homogeneous material with a uniform distribution of properties, stresses and strains. When an element of soil is tested in an apparatus, the uniform distribution of the properties, stresses and strains over the entire element can be lost and can be locally homogeneous. **Desrues et al. (1996)** showed for triaxial compression tests on sand that the void ratio in a shear band reached locally a unique value. However, the inclusion of these local phenomena in constitutive model requires dedicated features, which falls out of the scope of this chapter.

2. GENERAL FORMULATION

Many of the classical elasto-plastic constitutive models are based on decomposition of the deformation into reversible (elastic) and irreversible (plastic) components (**Eq. 1**).

$$d\tilde{\varepsilon} = d\tilde{\varepsilon}^e + d\tilde{\varepsilon}^p \qquad \text{Eq. 1}$$

where $d\tilde{\varepsilon}$, $d\tilde{\varepsilon}^e$ and $d\tilde{\varepsilon}^p$ are the total, elastic and plastic strain increment tensors, respectively.

The models use the concept of effective stresses (**Eq. 2**) which state that all changes in effective stresses result in changes in strains and vice-versa (**Eq. 3**).

$$\tilde{\sigma}' = \tilde{\sigma}^{tot} - p_w\tilde{\mathrm{I}} \quad \text{Eq. 2}$$

$$d\tilde{\sigma}' = \underline{D} \cdot d\tilde{\varepsilon} \quad \text{Eq. 3}$$

where $\tilde{\sigma}'$ is the effective stress tensor, $\tilde{\sigma}^{tot}$ is the total stress tensor, $p_w$is the pore water pressure, $\tilde{I}$ is the unit tensor and $\underline{D}$ is the fourth order stiffness matrix.

The elastic stiffness is defined by **Eq. 4** and the elastic stiffness matrix $\underline{D_e}$ for stress/strain vectors is given by Eq. **5**.

$$d\tilde{\sigma}' = \underline{D_e} \cdot d\tilde{\varepsilon}^e \quad \text{Eq. 4}$$

$$\underline{D_e} = \begin{bmatrix} K+4/3G & K-2/3G & K-2/3G & 0 & 0 & 0 \\ K-2/3G & K+4/3G & K-2/3G & 0 & 0 & 0 \\ K-2/3G & K-2/3G & K+4/3G & 0 & 0 & 0 \\ 0 & 0 & 0 & G & 0 & 0 \\ 0 & 0 & 0 & 0 & G & 0 \\ 0 & 0 & 0 & 0 & 0 & G \end{bmatrix} \quad \text{Eq. 5}$$

where *K* is the bulk modulus and *G* is the shear modulus.

The critical state framework **(Schofield and Wroth 1968)** assumes normality between the stress and strain increments following **Drucker et al. (1957)** (**Eq. 6**). It was motivated by the fact that normality was observed in experiments on clay specimens during the hardening phase (*i.e.* associated flow models) (Schofield and Wroth 1968).

$$d\tilde{\varepsilon}^p = \lambda \frac{\partial F}{\partial \tilde{\sigma}} \quad \text{Eq. 6}$$

where λ is the plastic multiplier and F the yield function which defines the boundary of the elastic domain. Constitutive models that adopt functions different from the yield function for plastic strain increments are available (*i.e.* non-associated flow models). Although this will provide more flexible and perhaps more realistic behaviour in terms of stress-strain relationships of certain soils, the associated flow models presented in this chapter still provide essential soil behaviour observed in experiments. Two critical state based models (Cam-clay and Nor-sand) will be presented in this chapter and they both have the following mathematical form (**Eq. 7**) for yield function.

$$F\left(\tilde{\sigma}, W_p\right) = 0 \quad \text{Eq. 7}$$

where W_p is a history variable, which stores information of the past deformation and can be a scalar, vector or tensor. It is often related to plastic strain $\tilde{\varepsilon}^p$; that is, $W_p(\tilde{\varepsilon}^p)$.

The following consistency condition implies that the stress state satisfies the yield criteria during plastic deformation (**Eq. 8**).

$$\dot{F}(\tilde{\sigma}, W_p) = \frac{\partial F}{\partial \tilde{\sigma}} d\tilde{\sigma} + \frac{\partial F}{\partial W_p} dW_p = \frac{\partial F}{\partial \tilde{\sigma}} d\tilde{\sigma} + \frac{\partial F}{\partial W_p} \frac{\partial W_p}{\partial \tilde{\varepsilon}^p} d\tilde{\varepsilon}^p = 0 \qquad \text{Eq. 8}$$

An incremental stress-strain equation (**Eq. 3**) can be developed by substituting **Eq. 1**, **Eq. 4** and **Eq. 6** into **Eq. 8**, and is given by **Eq. 9**. It is expressed in terms of the yield function F and the energy dissipation mechanism $\partial W_p / \partial \tilde{\varepsilon}^p$ which are intrinsic constituents of a constitutive model.

$$d\tilde{\sigma}' = \left[\underline{D_e} - \frac{\underline{D_e} \frac{\partial F}{\partial \tilde{\sigma}'} \left(\frac{\partial F}{\partial \tilde{\sigma}'} \right)^T \underline{D_e}}{\left(\frac{\partial F}{\partial \tilde{\sigma}'} \right)^T \underline{D_e} \frac{\partial F}{\partial \tilde{\sigma}'} - \frac{\partial F}{\partial W_p} \left(\frac{\partial W_p}{\partial \tilde{\varepsilon}^p} \right)^T \frac{\partial F}{\partial \tilde{\sigma}'}} \right] d\tilde{\varepsilon} \qquad \text{Eq. 9}$$

where the superscript T is the transpose function.

The Cam-Clay and Nor-Sand models presented in this chapter utilize the three stress invariants (mean effective stress p', the deviatoric stress q and the Lode angle θ) rather than the effective stress $\tilde{\sigma}'$, and were defined in **Chapter 1**. Therefore, the partial derivative of the yield function F with respect of $\tilde{\sigma}'$ yields to **Eq. 10**.

$$\frac{\partial F}{\partial \tilde{\sigma}'} = \frac{\partial F}{\partial p'} \frac{\partial p'}{\partial \tilde{\sigma}'} + \frac{\partial F}{\partial q} \frac{\partial q}{\partial \tilde{\sigma}'} + \frac{\partial F}{\partial \theta} \frac{\partial \theta}{\partial \tilde{\sigma}'} \qquad \text{Eq. 10}$$

The partial derivatives of the yield function are specific to each constitutive model. The partial derivatives of the stress variables are given in **Appendix A**.

The two constitutive models use a scalar as history variable W_p. The preconsolidation pressure p_c is used for Cam-Clay, whereas the image pressure p_i is used for Nor-Sand. The size of the yield surface is determined by the magnitude of these history variables, and can be function of plastic volumetric strain ε_v^p, plastic deviator strain ε_d^p or both.

The hardening/softening rule (**Eq. 11**) determines how the yield surface changes in shape or, in other words, how the elastic domain changes in size in the stress space. The partial

derivative of the yield function is specific to each constitutive model, and are given in this Chapter.

$$\frac{\partial F}{\partial W_p} = \frac{\partial F}{\partial p_{c\,(or\,i)}} = \frac{\partial F}{\partial p_c}\left(\frac{\partial p_{c\,(or\,i)}}{\partial \varepsilon_v^p}\frac{\partial \varepsilon_v^p}{\partial \bar{\varepsilon}^p} + \frac{\partial p_{c\,(or\,i)}}{\partial \varepsilon_d^p}\frac{\partial \varepsilon_d^p}{\partial \bar{\varepsilon}^p}\right) \quad \text{Eq. 11}$$

The energy dissipating mechanism is an assumption of the constitutive model. For instance, Cam-Clay assumes that the energy is dissipated by volumetric plastic strain ε_v^p, whereas Nor-Sand assumes that the energy is dissipated by plastic deviatoric strain ε_d^p. The partial derivatives of the strain variables are given in **Appendix A**.

3. CAM-CLAY

Cam-Clay is a simple elastic-plastic model for clays. It was the first model to capture the different mechanical behaviours from various stress and strain state conditions. Two versions of Cam-Clay exist – original Cam-Clay **(Roscoe and Schofield 1963)** and modified Cam-Clay **(Roscoe and Burland 1968).** Both models follow the same modelling principles but are formulated in a slightly different way. This will be illustrated in this section.

3.1 Yield function

Original Cam-Clay find its roots in **Taylor's (1948)** stress-dilatancy equation based on the work balance (**Eq. 12**), discussed in **Chapter 1 Section 4**, from which it is possible to formulate a flow rule (**Eq. 13**). It is expressed in terms of effective stress ratio $\eta' = q/p'$, the critical state stress ratio M and the dilatancy rate $D = d\varepsilon_v^p / d\varepsilon_d^p$.

$$p' d\varepsilon_v^p + q\, d\varepsilon_d^p = p' M d\varepsilon_d^p \quad \text{Eq. 12}$$

$$\rightarrow \eta' = M - D \quad \text{Eq. 13}$$

Roscoe and Schofield (1963) used the associated flow rule by means of the following normality equation following the work of **Drucker et al. (1957)**.

$$\frac{dq}{dp'} \cdot \frac{d\varepsilon_d^p}{d\varepsilon_v^p} = -1 \quad \text{Eq. 14}$$

It is then possible to substitute Eq. **14** into Eq. **13**, which gives Eq. **15**.

$$q = Mp' + p' \frac{dq}{dp'} \qquad \text{Eq. 15}$$

The deviatoric stress q can be expressed as $q = \eta' p'$ and substituted in Eq. **15**, which gives Eq. **16**.

$$\rightarrow \eta' p' = Mp' + p' \frac{d(\eta' p')}{dp'} \qquad \text{Eq. 16}$$

The development of Eq. **16** gives Eq. **17**.

$$\rightarrow \eta' = M + \frac{d\eta'}{dp'} p' + \eta'$$

$$\rightarrow \frac{dp'}{p'} = -\frac{d\eta'}{M} \qquad \text{Eq. 17}$$

The integration of Eq. **17** with the known point ($p' = p_c,\ q = 0,\ \eta' = 0$) gives **Eq. 18**, as shown in Figure 1a in the (p'- q) space. The equation forms a curve on which the soil yields and exhibits an elasto-plastic behaviour. It is known as Original Cam-Clay's yield surface.

$$\rightarrow \eta' = M \cdot \ln\left(\frac{p_c}{p'}\right) \qquad \text{Eq. 18}$$

where p_c is the preconsolidation pressures and sizes the yield function.

The yield surface can be expressed as a function as shown in **Eq. 19**. The yield function is illustrated in **Figure 1 (a).** When the soil has an elastic behaviour, its stress state is located within the yield surface and the yield function is negative ($F < 0$). When the soil has an elastic-plastic behaviour, its stress state is located on the yield surface ($F = 0$). The stress is necessarily located within or on the yield surface and no stress states can be located outside the yield surface.

Original Cam Clay: $$F = \eta' - M \cdot \ln\left(\frac{p_c}{p'}\right) \qquad \text{Eq. 19}$$

The relationship between the history variable p_c and the corresponding critical state pressure p_{cs} is $\ln(p_c/p_{cs}) = 1$.

The yield function of original Cam-Clay has as singularity at the tip of yield surface ($p' = p_c, q = 0$) for which the strain increment is undefined along the isotropic stress path (increasing $p'$with q =0). **Roscoe and Burland (1968)** suggested a different energy

dissipating mechanism which included the volumetric strain as a dissipating mechanism (**Eq. 20**). The development of this equation, in the same way as original Cam-Clay was developed, gives an elliptic shape (**Eq. 21**). This version of the model is referred to as modified Cam-Clay, and the shape of the yield function is an ellipse as shown in **Figure 1 (b).**

$$p' d\varepsilon_v^p + q\, d\varepsilon_d^p = p' \sqrt{\left(d\varepsilon_v^p\right)^2 + \left(M d\varepsilon_d^p\right)^2} \qquad \text{Eq. 20}$$

Modified Cam-Clay: $$F = \left(\frac{\eta'}{M}\right)^2 + (p' - p_c) \qquad \text{Eq. 21}$$

The relationship between the history variable p_c and the corresponding critical state pressure p_{cs} is $p_c/p_{cs} = 2$.

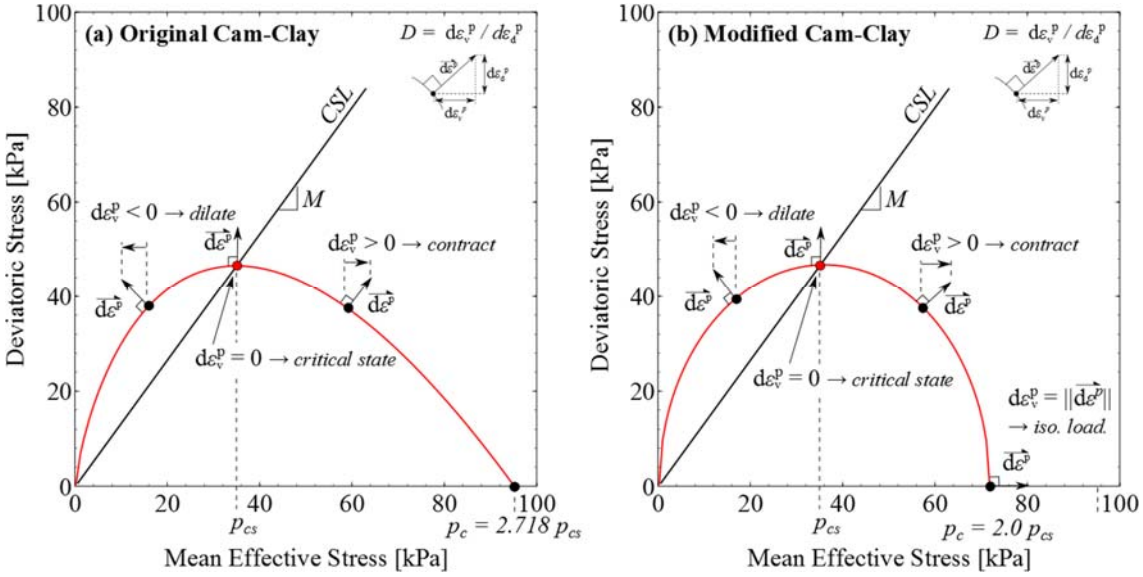

Figure 1: Yield surfaces of (a) original Cam-Clay and (b) modified Cam-Clay

The yield surfaces are defined by $p'$and q and hence the partial derivatives of $\partial F/\partial p'$ and $\partial F/\partial q$ for original Cam-Clay (**Eq. 19**) and modified Cam-Clay (**Eq. 21**) can be computed and are given in **Eq**. 22 to **Eq**. 27**.**

Original Cam-Clay

$$\frac{\partial F}{\partial p'} = M\left[1 - \ln\left(\frac{p_c}{p'}\right)\right] \qquad \text{Eq. 22}$$

$$\frac{\partial F}{\partial q} = 1 \qquad \text{Eq. 24}$$

$$\frac{\partial F}{\partial p_c} = -M\frac{p'}{p_c} \qquad \text{Eq. 26}$$

Modified Cam-Clay

$$\frac{\partial F}{\partial p'} = 2p' - p_c \qquad \text{Eq. 23}$$

$$\frac{\partial F}{\partial q} = 1 \qquad \text{Eq. 25}$$

$$\frac{\partial F}{\partial p_c} = -p' \qquad \text{Eq. 27}$$

As discussed in **Chapter 1**, the critical state angle M is a function of Lode angle θ, and its partial derivative $\partial F/\partial\theta$ is given by **Eq. 28**.

$$\frac{\partial F}{\partial \theta} = \frac{\partial F}{\partial M}\frac{\partial M}{\partial \theta} \qquad \text{Eq. 28}$$

The partial derivative $\partial F/\partial M$ is specific to the constitutive model, and is given in **Eq. 29** and **Eq. 30** for original and modified Cam-Clay, respectively.

Original Cam-Clay

$$\frac{\partial F}{\partial M} = -\ln\left(\frac{p_c}{p'}\right) \qquad \text{Eq. 29}$$

Modified Cam-Clay

$$\frac{\partial F}{\partial M} = 2\frac{\eta'^2}{M^3} \qquad \text{Eq. 30}$$

The dependency of the critical state stress ratio M with the Lode angle θ is modelled separately as described in **Chapter 1**. Its partial derivative can be obtained consequently.

3.2 Volume Change Behaviour and Stress-Dilatancy

For illustration purpose, the volumetric plastic strain increment $d\varepsilon_v^p$ and the deviatoric plastic strain increment $d\varepsilon_v^p$ are co-assigning to the horizontal axis and vertical axis, respectively. The normality condition between the strains and the stresses implies that the strain increment is normal to the yield surface as illustrated in **Figure 1.**

The critical state theory **(Roscoe et al. 1958)** suggests that a logarithmic relationship exists between the mean critical state effective stress p'_{cs} and the specific volume v at critical state (**Eq. 31**), and shown in **Figure 2**.

$$v_{cs} = \Gamma - \lambda \ln(p'_{cs}) \qquad \text{Eq. 31}$$

where $v_{cs} = 1 + e_{cs}$ is the critical state specific volume, Γ the critical state specific volume at 1kPa pressure and λ the critical state slope.

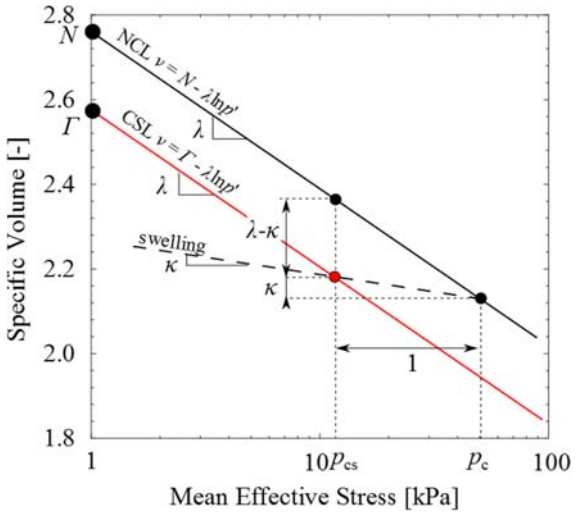

Figure 2: Critical state and normal consolidation lines as proposed in Cam-Clay

When the stress ratio state on the yield surface is smaller than the critical state stress ratio ($\eta' < M$), the volumetric strain increment is positive for a given deviator strain increment. The soil is contractive and the state of the soil is located above the critical state line (**Eq. 31)** in the $(v - \ln p')$ space. When the stress ratio state on the yield surface is larger than the critical state stress ratio ($\eta' > M$), the volumetric strain increment is negative from the stress dilatancy relationship and the soil dilates. When the stress state is located at the summit of the yield function ($\eta' = M$), the soil is at critical state and the volumetric strain increment is nil (that is, the plastic strain vector in **Figure 1 (a)** is in the vertical direction). Therefore, no changes in volume occur and the dilatancy is nil as the soil is on the critical state line.

Both the original and modified Cam-Clay models assume that the plastic (or virgin) consolidation by isotropic compression is parallel to the critical state line, as shown in **Figure 2**. This is often called the normal compression line (NCL), which is defined by **Eq. 32.**

$$v = N - \lambda \ln(p') \qquad \text{Eq. 32}$$

where $v = 1 + e$ is the specific volume and N the 'isotropic' density at 1 kPa pressure.

During an isotropic compression tests, the stress and strain state of the soil evolve along the normal compression line. The size of the yield surface increases and the isotropic stress path gives $p' = p_c$ as shown in **Figure 2**.

When the soil is unloaded, it exhibits elastic behaviour and expands. This expansion is characterised by elastic swelling, and is modelled in Cam-Clay as shown by **Eq. 33**.

$$v = v_c - \kappa \ln\left(\frac{p'}{p_c}\right) \qquad \text{Eq. 33}$$

where $v_c$is the specific volume prior to unloading. κ is the swelling index, which is the slope of the swelling line in the $v - \ln p'$ space.

The position of the normal compression line in relation to the critical state line is given by the yield function and the values of λ and κ. This yields to **Eq. 34** and **Eq. 35** for original and modified Cam-Clay, respectively.

Original Cam-Clay

$N = \Gamma + \lambda - \kappa$ Eq. 34

Modified Cam-Clay

$N = \Gamma + (\lambda - \kappa) \cdot ln2$ Eq. 35

During isotropic compression, the material hardens and the yield surface grows. Both Cam-Clay models assume that the rate of increase of the yield surface follows the normal compression line. Therefore, the hardening is driven by plastic volumetric strain only (*i.e.* $\partial p_c / \partial \varepsilon_d^p = 0$) and the hardening law is expressed by **Eq. 36**, which can be derived geometrically from Figure 2.

$$\frac{\partial p_c}{\partial \varepsilon_v^p} = \frac{v}{\lambda - \kappa}\, p_c \qquad \text{Eq. 36}$$

3.3 Elasticity

When the stress state is inside the yield surface, it is assumed that the mechanical behaviour is elastic. In the current implementation of the Cam-Clay models presented in this chapter, the elastic behaviour is considered to be isotropic and hence two parameters (elastic bulk modulus K_e and Poisson's ratio ν^e) are needed. Poisson's ratio ν^e is assumed to be constant. It is denoted by the Greek letter '*nu*' and the postscript '*e*' for elastic in order to avoid confusing with the specific volume denoted with the roman letter 'v'.

It can be shown that the bulk modulus is dependent on the swelling modulus κ, the mean pressure p' and the specific volume v (Eq. **37**), by using the κ-line swelling model and differentiating it.

$$K^e = \frac{\delta p'}{\delta \varepsilon_v^e} = \frac{\delta p'}{\delta v} v = \frac{v p'}{\kappa} \qquad \text{Eq. 37}$$

The two elastic parameters $K^e$and ν^e are used to build the elastic stiffness matrix $\underline{D_e}$ of Eq. 5.

By substituting appropriate equations defined above into Eq. **9**, the incremental form of Cam-Clay strain-strain models can be derived. The numerical implementation in MATLAB of both original and modified Cam-Clay can be obtained from the publisher's website.

3.4 Simulations of Drained Triaxial Compression Tests

Figure 3 and **Figure 4** show the simulation results of triaxial compression tests with the original and the modified Cam-Clay models using the parameters given in **Table 1**. The simulations were run by consolidating a clay specimen to an initial isotropic mean effective stress of 20 kPa and then sheared in triaxial compression both in drained and undrained conditions. The results from the drained tests are shown in this section, whereas those from the undrained tests are shown in the next section.

Table 1: Cam-Clay Model parameters and initial conditions for simulations

κ	ν	M	λ	N	p'	$p_c{}^*$
0.062	0.2	0.89	0.161	2.76	20 kPa	100 kPa

** for overconsolidated specimens. Γ is calculated in the model (Eq. 34 and Eq. 35).*

The triaxial compression test is a conventional laboratory test in which a cylindrical soil sample is consolidated by isotropic pressure and is then sheared by increasing the axial stress but keeping the radial stress constant. A drained test implies that the pore water pressure is kept constant during axial compression and the specimen volume can change by allowing the pore water to move in or out of the specimen. Hence, the total stress increment is equal to the effective stress increment; that is, the excess pore pressure is zero.

A normally consolidated state implies that the sample has never been subjected to a higher pressure. The initial mean effective stress p' is the preconsolidation pressure p_c as shown by point A in **Figure 3 (a)** and **Figure 4 (a)**. It is on the 'wet' side of the critical state line as its initial water content is higher than its critical state value. The drained triaxial compression ($d\sigma'_1 > 0, d\sigma'_3 = 0$) imposes an effective stress path with a stress ratio rate of $dq/dp' = d\sigma'_1/(d\sigma'_1/3) = 3$ as shown in the figures.

As the material is sheared with the given stress path, the mobilised shear resistance increases in a non-linear manner until reaching the critical state line, and the specific volume decreases from the normal compression line to the critical state line. This phase is known as the

hardening phase, in which the yield surface grows until the stress state is located at the summit of the yield surface and on the critical state line. Accordingly, the preconsolidation pressure p_c increases. For a given set of model parameters, Modified Cam-Clay predicts a stiffer response than original Cam-Clay and this is due to the difference in yield surface shape.

Overconsolidated samples have been previously isotopically loaded and then unloaded before any shearing takes place. Therefore, the yield surface expands during the loading phase with $p' = p_c$. The sample is then unloaded and behaves elastically along the κ-line. That is, the yield surface remains at its position by keeping the value of p_c but the unloaded stress state is located within the yield surface ($p' < p_c$). This state corresponds to point A in **Figure 3 (b)** and **Figure 4 (b).** The overconsolidation densifies the material and its initial specific volume prior to shearing can be located below the critical state line if the unloaded pressure is much smaller than the preconsolidation pressure (*i.e.* $\ln(p_c/p') > 1$ for original Cam-Clay and $p_c/p' > 2$ for modified Cam-Clay). The state of the soil is on the 'dry' side of the critical state.

When the heavily overconsolidated sample is sheared in drained conditions with the triaxial compression stress path of $dq/dp' = 3$, the sample initially exhibits elastic behaviour from point A to point B crossing the critical state line. It does not reach a critical state because the soil is elastic and the specific volume state is not on the critical state line. The soil contracts during this elastic phase due to increase in mean pressure p'.

The soil then yields when the stress state reaches the yield surface as shown in **Figures 3 (a)** and **Figure 4 (a)** and this corresponds to the peak shear resistance (point B). Original Cam-Clay (**Figure 3 b**) predicts a lower peak strength than Modified Cam-Clay (**Figure 4 b**) for the same preconsolidation pressure p_c. This is due to the different shapes of the yield function. As from this point, the soil behaves as an elastic-plastic material. As the stress ratio state at yield is greater than the critical state ($\eta' > M$) for heavily overconsolidated clay, it dilates and at the same time softens to reach to the critical state by keeping the stress path of $dq/dp' = 3$. Therefore, the shear resistance decreases as shearing continues and then finally reaches to the critical state when the stress ratio becomes $\eta = M$ and the specific volume is on the critical state line in the $(v - \ln p')$ plane. The yield surface shrinks and the preconsolidation pressure p_c decreases (i.e. softening).

3.3 Simulations of Undrained Triaxial Compression Tests

Triaxial tests can also be run in undrained conditions. It means that no pore water can flow in or out of the sample. The water is relatively incompressible and hence the sample volume is kept constant throughout the test during shearing. Triaxial compression tests will give the total stress path to be $dq/dp = 3$, but the effective stress path will not follow $dq/dp' = 3$ due to excess pore pressure generation. The magnitude of excess pore pressure depends on the dilative or contractive nature of the sample.

Figure 3 (c) and **Figure 4 (c)** illustrates the triaxial compression case of a normally consolidated clay sample in undrained conditions. The constant volume condition implies that the mean effective stress state of the clay needs to move from point A to point B in the horizontal direction of the $(v - \ln p')$ plane in order to reach to the critical state of $p_{cs(B)}$. Positive excess pore pressure develops during shearing and the shear resistance at the critical state becomes $q_{cs(B)}$ as shown in the figure. The effective stress path moves to the upper left direction in the $(p' - q)$ space and the path can be evaluated from the incremental stress-strain relationship with the constant volume constraint ($d\varepsilon_v = 0$), as shown by Eq. **38**.

$$d\varepsilon_v = d\varepsilon_v^e + d\varepsilon_v^p = \frac{dp'}{K^e} + d\varepsilon_v^p = 0 \qquad \text{Eq. 38}$$

$$\rightarrow\ dp' = -K^e d\varepsilon_v^p \qquad \text{Eq. 39}$$

Eq. **39** shows that the contractive tendency of the clay ($d\varepsilon_v^p > 0$) decreases the mean effective stress.

The soil hardens and the preconsolidation pressure increases from $p_{c(A)}$ to $p_{c(B)}$. However, the degree of hardening is much smaller than the drained case in **Figure 3 (a)** and **Figure 4 (a).** Hence, in triaxial compression condition, the undrained shear strength of normally consolidated clay is smaller than the drained shear strength.

Figure 3 (d) and **Figure 4 (d)** illustrate the triaxial compression case of a heavily overconsolidated sample in undrained conditions. The stress-strain path differs largely from the one observed for the normally consolidated sample. The overconsolidation increases the

size of the yield surface and the sample initially undergoes elastic deformation from point A to point B. In undrained condition, the mean effective stress remains constant ($dp' = 0$) as the deviatoric stress q increases during elastic deformation ($d\varepsilon_v = d\varepsilon_v^e = 0$). This is because $dp' = K_e d\varepsilon_v^e = 0$.

Once the stress state reaches the yield surface at point B, the soil yields and becomes elasto-plastic. As the soil is on the dry side of the critical state line, the effective stress state needs to move to the right direction from Point B to Point C in the ($v - \ln p'$) plane so that the constant volume condition (dv = 0) can be kept. The clay has a dilative tendency ($d\varepsilon_v^p < 0$) and hence the effective mean pressure increases with shearing ($dp' > 0$) according to Eq. **39**. The mean pressure at the critical state in undrained condition is greater than that in drained condition. Hence, the undrained shear strength of heavily overconsolidated clay is greater than the drained shear strength in the triaxial compression case.

3.6 Remarks on Cam-Clay

Both original and modified Cam-Clays provide a simple mathematical idealisation of the mechanical behaviour of clay and were revolutionary at the time. When predicting the behaviour of 'dry' soil, it behaves elastically and then suddenly becomes plastic. The peak strength is the consequence of the overconsolidation imposed by these models. Real clays show more gradual transition from elastic to plastic behaviour and hence it can be argued that the peak strength is associated with dilation characteristics of the clay rather than a pure sudden changes from elastic to elasto-plastic.

Cam-Clay predicts contraction when the dilatancy rate is positive, and dilation when the dilatancy rate is negative. The associated hardening and softening behaviour is controlled by the hardening rule ($\partial F / \partial \varepsilon_v^p$). The critical state is reached when the dilatancy rate and hence the hardening rule are nil. For this reason, the Cam-Clay models are said to be formulated on the first condition of the critical state theory ($D = 0$). It does not give the second condition of the critical state theory ($\partial D / \partial \varepsilon_d^p = 0$) explicitly in the formulation.

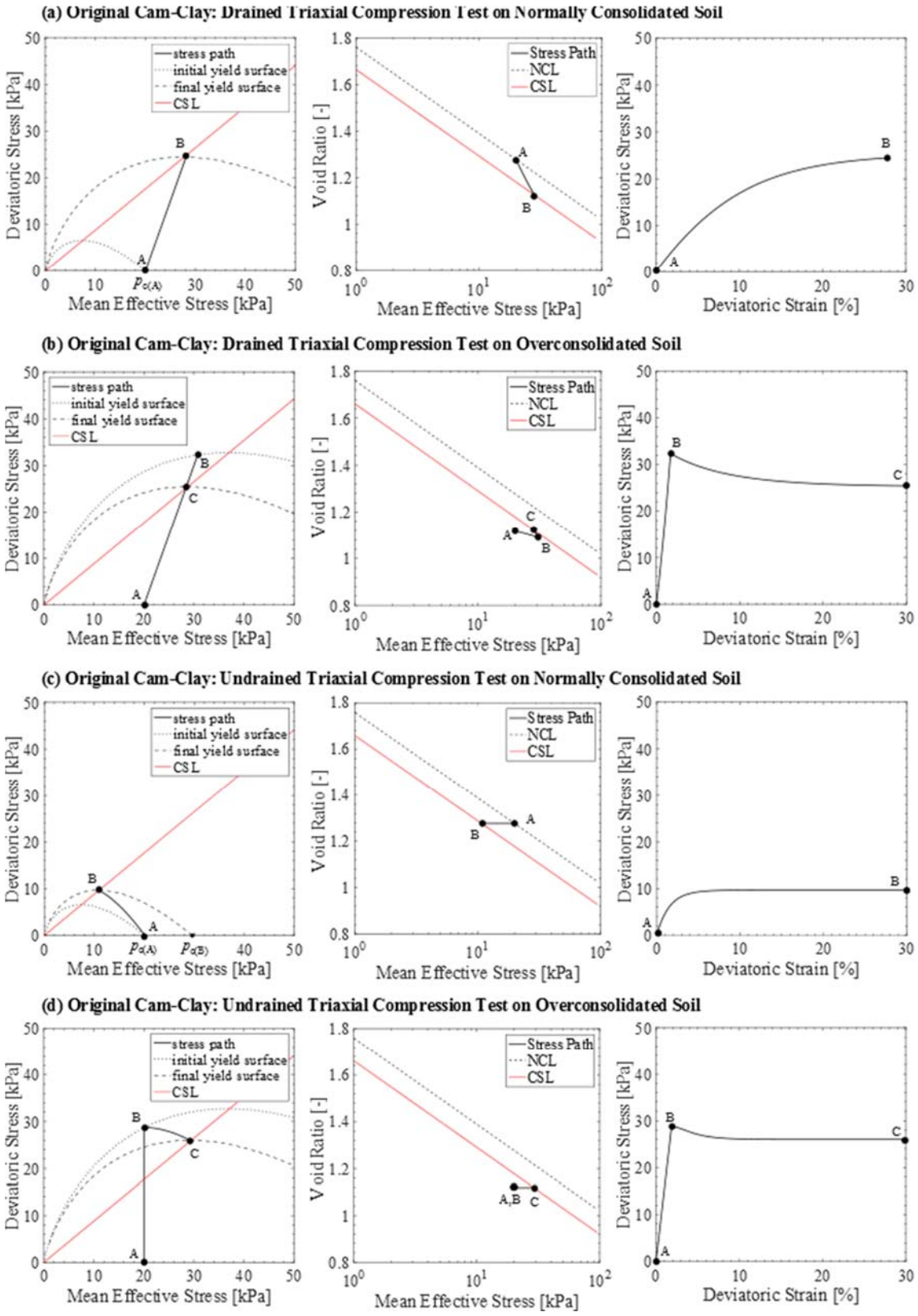

Figure 3: Triaxial compression simulations with Original Cam-Clay

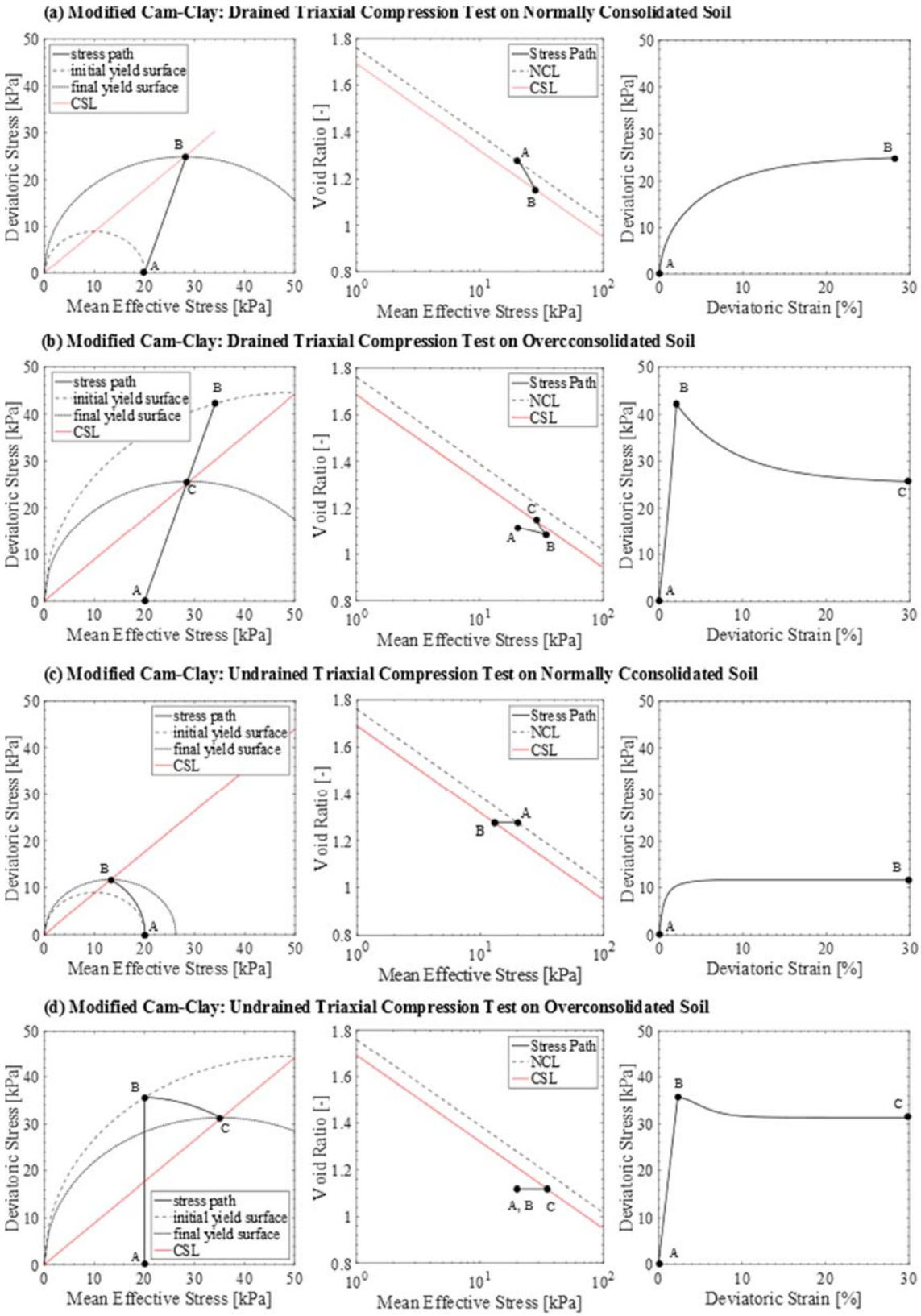

Figure 4: Triaxial compression simulations with Modified Cam-Clay

4. SUB-LOADING SURFACE MODEL

4.1 General framework

It was shown in the previous section that the introduction of plastic strains was determined by the yield surface and that this yield surface determined the peak state for heavily overconsolidated cases. **Hashiguchi (1979)** and **Hashiguchi and Chen (1998)** introduced a new surface called the *sub-loading surface*. It allows plastic strains to take place prior to the stress state reaching the yield surface and is formulated on the second condition of the critical state theory ($\partial D/\partial \varepsilon_d^p = 0$).

The sub-loading surface defines the elastic domain and function as the classical yield surface, in which the stress state can only be within the sub-loading surface (elastic) or on the sub-loading surface (elasto-plastic). The classical yield surface sized by p_c now becomes the limit yield surface. The sub-loading surface is smaller or equal to the outer limit yield surface and hence the consolidation pressure p_c^{SL} sizing the sub-loading surface can be formulated as show by Eq. **40**.

$$p_c^{SL} = R \cdot p_c \quad \text{with } R \leq 1 \qquad \text{Eq. 40}$$

where R is the preconsolidation pressure ratio. The sub-loading surface and the yield surface are illustrated in **Figure 5.**

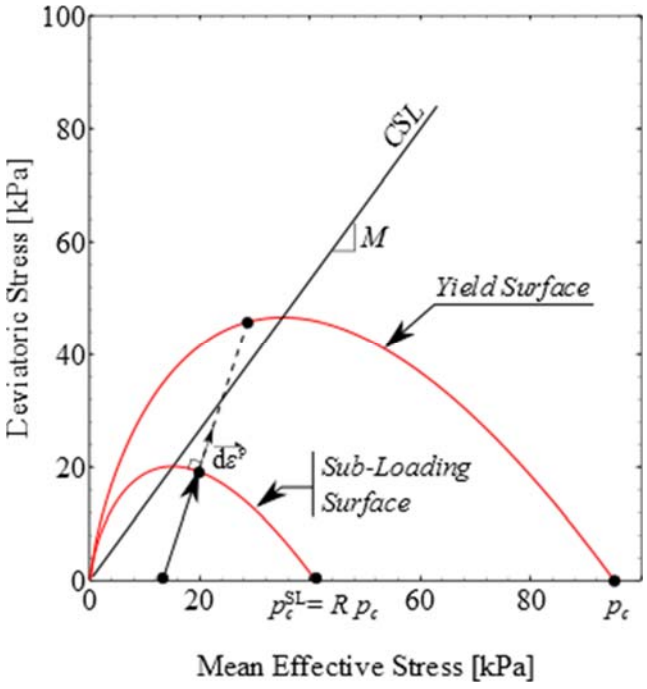

Figure 5: Yield and sub-loading surfaces

Hashiguchi and Chen (1998) suggested formulating a constitutive model in terms of the sub-loading surface (Eq. **40**). The inclusion of the new variable R causes a modification of the consistency condition (Eq. **41**), which adds a new hardening term in the incremental stress strain equation (Eq. **42**).

$$\dot{F}(\tilde{\sigma}, W_p) = \frac{\partial F}{\partial \tilde{\sigma}} d\tilde{\sigma} + \frac{\partial F}{\partial W_p} dW_p + \frac{\partial F}{\partial R} dR = 0 \qquad \text{Eq. 41}$$

$$\rightarrow d\tilde{\sigma}' = \left[\underline{D_e} - \frac{\underline{D_e} \frac{\partial F}{\partial \tilde{\sigma}'} \left(\frac{\partial F}{\partial \tilde{\sigma}'}\right)^T \underline{D_e}}{\left(\frac{\partial F}{\partial \tilde{\sigma}'}\right)^T \underline{D_e} \frac{\partial F}{\partial \tilde{\sigma}'} - \frac{\partial F}{\partial W_p} \left(\frac{\partial W_p}{\partial \tilde{\varepsilon}^p}\right)^T \frac{\partial F}{\partial \tilde{\sigma}'} - \frac{\partial F}{\partial R} \left\| \frac{\partial F}{\partial \tilde{\sigma}'} \right\| dR} \right] d\tilde{\varepsilon} \qquad \text{Eq. 42}$$

Two hardening terms are expressed - one for the yield surface $\left(-\frac{\partial F}{\partial W_p}\left(\frac{\partial W_p}{\partial \tilde{\varepsilon}^p}\right)^T \frac{\partial F}{\partial \tilde{\sigma}'}\right)$ and one for the sub-loading surface $\left(-\frac{\partial F}{\partial R}\left\|\frac{\partial F}{\partial \tilde{\sigma}'}\right\| dR\right)$. The first hardening term expresses the nil dilatancy condition at critical sate ($D = 0$) and the second hardening term expresses the nil changes in dilatancy at critical state ($\partial D / \partial \varepsilon_d^p = 0$). Therefore, these two conditions are

decoupled and permit plastic strains to develop in the hardening phase. This was not the case with the Cam-Clay models.

The change in the preconsolidation pressure ratio dR has to be explicitly expressed and must fulfil the following conditions when plasticity takes place ($d\varepsilon_d^p > 0$).

$R = 0 \quad \rightarrow dR = +\infty$

$0 < R < 1 \quad \rightarrow dR > 0$

$R = 1 \quad \rightarrow dR = 0$

$R > 1 \quad \rightarrow dR < 0$

Among different expressions, **Hashiguchi and Chen (1998)** suggested Eq. **43**.

$$dR = U \cdot (R^{-m} - 1) \qquad \text{Eq. 43}$$

where U and m are two model parameters controlling the brittleness of the stress-strain behaviour.

Figure 6 illustrates a drained triaxial compression test simulation with the sub-loading surface model. **Figure 6 (a)** shows the stress path, sub-loading surfaces and yield surfaces. **Figure 6 (b)** shows the development of strength, whereas **Figure 6 (c)** shows the volumetric behaviour. When the soil is sheared, the soil goes from point A to B, which is called the *phase transition point* (Tatsuoka et al., 1986). The dilatancy is nil ($D = 0$) because the mean effective stress is on the summit of the sub-loading surface, but the changes in dilatancy are not ($\partial D / \partial \varepsilon_d^p \neq 0$) because $dR \neq 0$. Therefore, the soil continues to harden until it reaches the peak state at point C, where the dilatancy rate is minimum and the deviator stress maximum. The soil then softens until it reaches point D, where it is at critical state ($D = 0$, $\partial D / \partial \varepsilon_d^p = 0$) because $p' = p'_{cs}$and $dR = 0$.

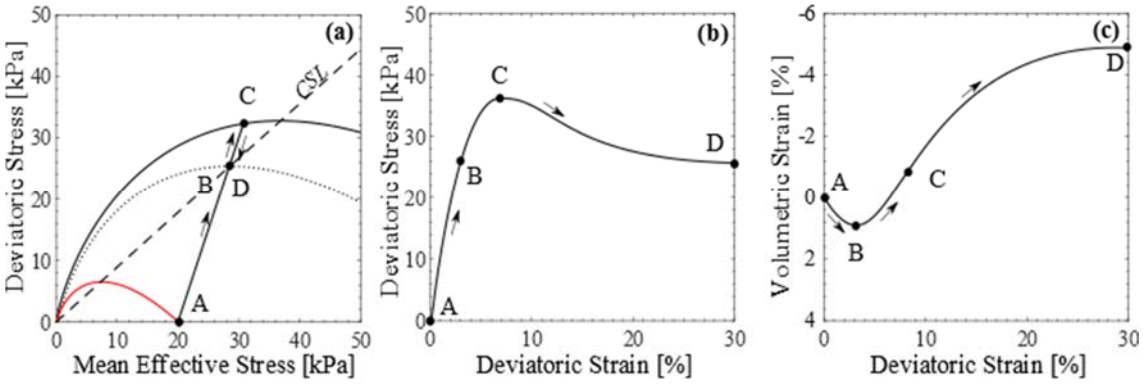

Figure 6: Schematic description of the sub-loading surface

4.2 Application to Original Cam-Clay

The preconsolidation pressure of the yield surface p_c is formulated as a function of the preconsolidation pressure of the sub-loading surface p_c^{sl} (Eq. **40**). Therefore, the yield function yields to Eq. **44**.

$$F = \eta' - M \cdot \ln\left(\frac{R \cdot p_c^{sl}}{p'}\right) \qquad \text{Eq. 44}$$

The partial derivatives of the yield function are obtained in exactly the same way as for the original model and are given in Eq. **45** to Eq. **47**.

$$\frac{\partial F}{\partial p'} = M\left[1 - \ln\left(\frac{R \cdot p_c^{sl}}{p'}\right)\right] \qquad \text{Eq. 45}$$

$$\frac{\partial F}{\partial q} = 1 \qquad \text{Eq. 46}$$

$$\frac{\partial F}{\partial M} = -\ln\left(\frac{R \cdot p_c^{sl}}{p'}\right) \qquad \text{Eq. 47}$$

$$\frac{\partial F}{\partial p_c^{sl}} = -M\frac{p'}{p_c^{sl}} \qquad \text{Eq. 48}$$

The yield function needs to be derived with respect to the preconsolidation pressure ratio R and is given by Eq. **49**.

$$\frac{\partial F}{\partial R} = -\frac{Mp'}{R} \qquad \text{Eq. 49}$$

The model has been implemented in MATLAB and the source code is available from the publisher's website.

Figure 7 illustrates the model in triaxial compression tests. The model parameters and initial states are given in **Table 2.**

Table 2: Cam-Clay Model with sub-surface loading parameters and initial conditions for simulations

κ	ν	M	λ	N	U	m	p'	$p_c{}^*$
0.062	0.2	0.89	0.161	2.76	200	0.2	20 kPa	250 kPa

** for overconsolidated specimens. Γ is calculated in the model (Eq. 34).*

4.3 Simulations of Drained Triaxial Compression Tests

Figure 7 (a) shows the simulation results of a drained triaxial compression test of a normally consolidated 'wet' clay specimen. The behaviour is identical as that of the original Cam-Clay model. The initial yield surface is on the sub-loading surface ($R = 1$) and both R and p_c grow simultaneously until reaching the critical state. This means that the two conditions of the critical state theory ($D = 0,\ \partial D/\partial \varepsilon_d^p = 0$) are fulfilled simultaneously by $p' = p'_{cs}$and $dR = 0$.

Figure 7 (b) shows the simulation results of a drained triaxial compression test of a 'dry' heavily overconsolidated clay. The behaviour is significantly different from that of the Original Cam-Clay model. The initial stress state is located on the sub-loading surface. The limit yield surface is larger than the sub-loading surface ($0 < R < 1$). During the first part of the hardening phase ($\eta' < M$) , the soil contracts despite being 'dry' (point A to B) as the stress state on the subloading surface gives contraction behaviour. At point B, it reaches the phase transition point, where the dilatancy rate is nil but the change in dilatancy is not ($D = 0,\ \partial D/\partial \varepsilon_d^p \neq 0$) because $dR \neq 0$. Therefore, the clay is not at critical state. It continues its hardening until reaching the peak strength at point C. During this second hardening phase, the clay dilates and reaches the minimum dilatancy rate at the peak state - point C. This is consistent with the stress-dilatancy theory. It is interesting to note that the peak state (point C) is not located on the initial limit yield surface. During the hardening phase, plastic deformation is permitted and the plastic work causes softening of the initial limit yield

surface. At the peak state, the sub-loading surface and the limit yield surface are on top of each other ($R = 1$) and remains so until the end of the test. The soil then softens from point C to B'. During this phase, the soil is still dilating but its rate is progressively reduced until reaching a nil dilatancy state at critical state, controlled by the yield surface ($p' = p'_{cs}$), and a nil dilatancy change, controlled by the sub-loading surface ($dR = 0$).

4.4 Simulations of Undrained Triaxial Compression Tests

Figure 7 (c) shows the simulation results of an undrained triaxial compression test of a 'wet' normally consolidated clay specimen. As for the drained case, the initial limit yield surface and the sub-loading surface are the same ($R = 1$). Therefore, the behaviour is identical to that of the Original Cam-Clay model.

Figure 7 (d) shows the simulation results of an undrained triaxial compression test of a 'dry' heavily overconsolidated clay specimen. The initial stress state is located on the sub-loading surface and the initial limit yield surface is larger than the sub-loading surface ($R < 1$). As the clay is sheared, it exhibits a rapid increase in shear resistance. During this phase, the clay has a contraction tendency and positive excess pore pressure develops. The clay gradually changes its behaviour to dilative one. The excess pore water pressure starts to decrease and becomes nil and even negative. During this phase the shear resistance increases due to increasing mean effective stress. It reaches a progressive peak state where the sub-loading surface and the yield surface coincide ($R = 1$). The clay then softens, albeit limited, until reaching the critical state.

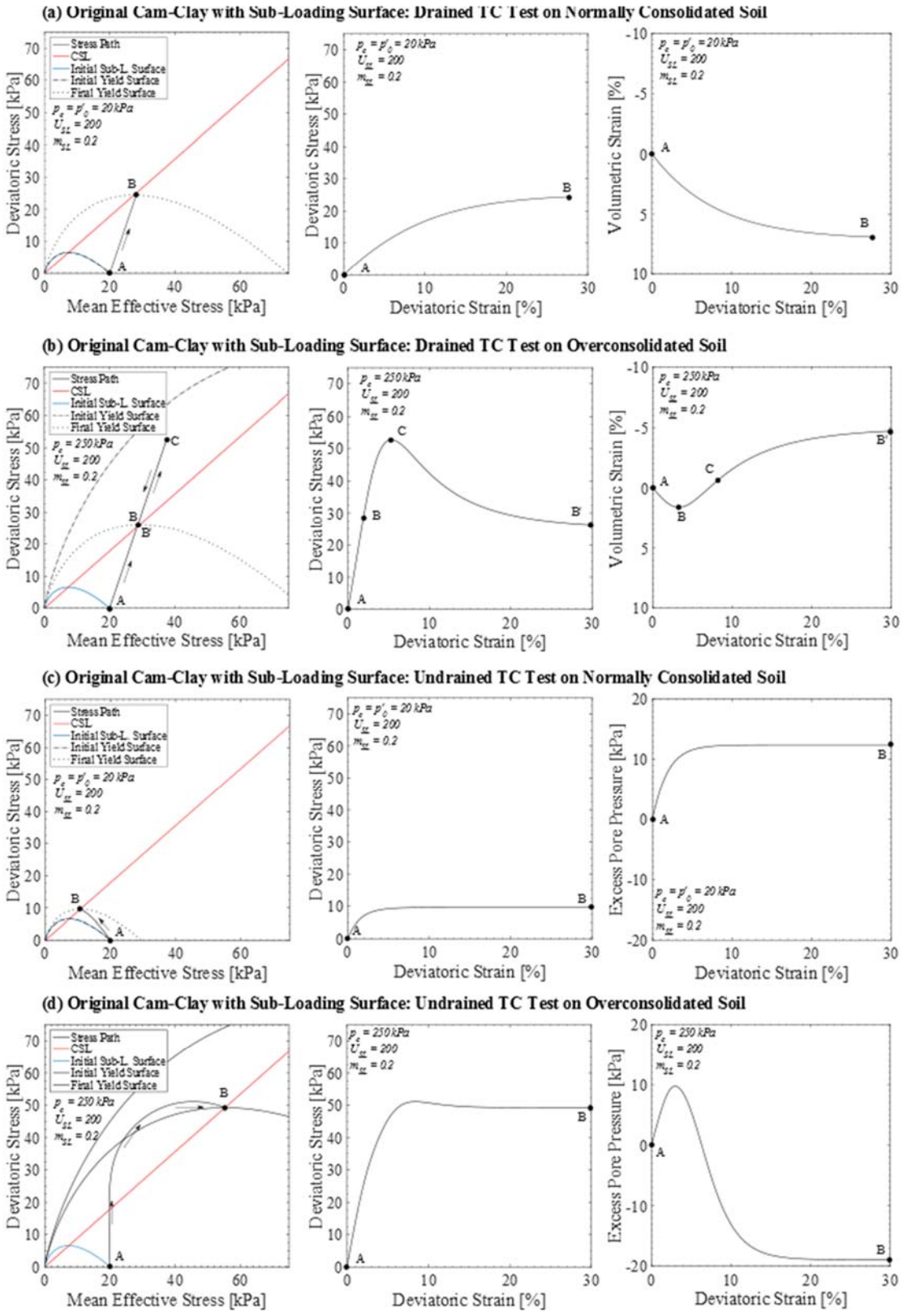

Figure 7: Triaxial compression simulations with Original Cam-Clay with Sub-Loading Surface

Two additional model parameters are necessary for the sub-loading surface model – U and m. These parameters do not have any physical meaning and cannot be experimentally quantified. However, they control the development of plastic deformation inside the yield surface. **Figure 8** shows the results of a series of sensitivity analysis on a heavily overconsolidated clay with an initial consolidation pressure p_c of 250 kPa (OCR = 12.5). The results show that these parameters affect mostly on the stiffness and slightly the dilatancy rate. They control the amount of plastic work and hence change the peak state.

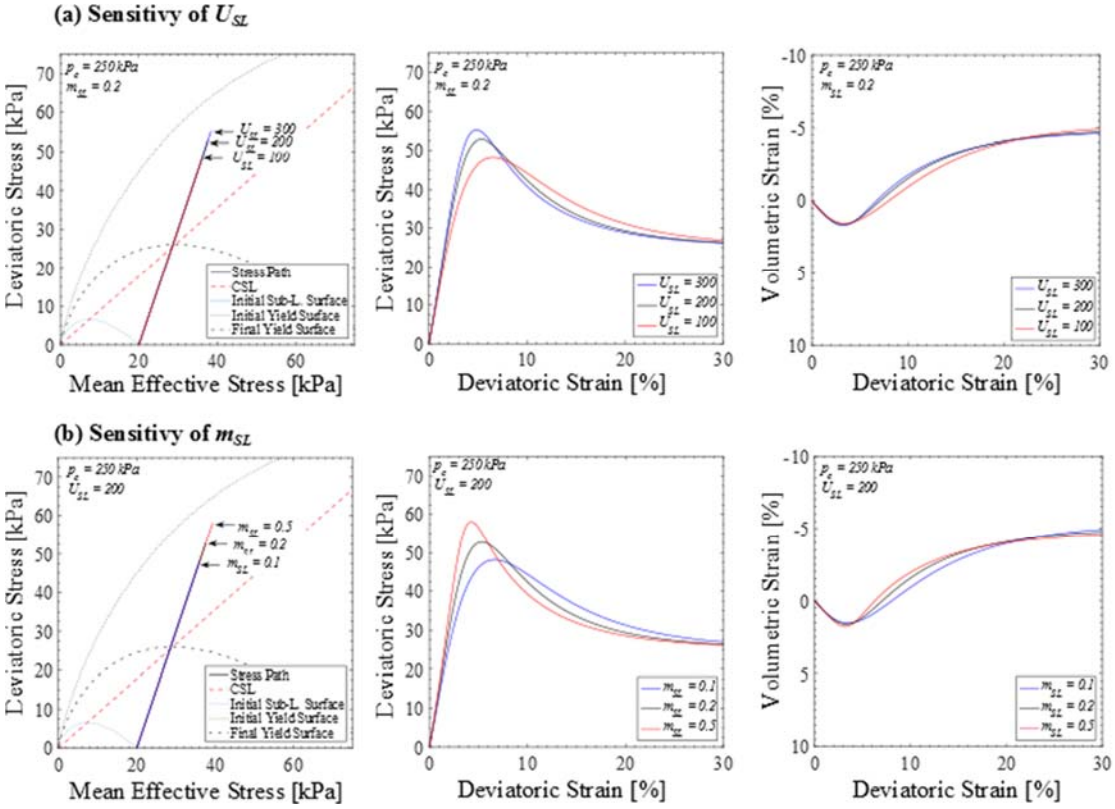

Figure 8: Sensitivity analysis on the sub-loading surface parameters

4.5 Remarks on Original Cam-Clay with sub-Loading surface concept

Whilst the behaviour of a 'wet' normally consolidated clay is identical to the classical formulation of the Original Cam-Clay Model, the behaviour of a 'dry' heavily overconsolidated clay is significantly improved in a simple manner using the sub-loading surface concept. The introduction of the sub-loading surface provides the second condition of the critical state theory in the model ($D = 0,\ \partial D/\partial \varepsilon_d^p = 0$), which in turn allows modelling of the phase transition behaviour. Furthermore, the stress-strain paths are continuous and

smooth without any singularities or abrupt changes. Therefore, the introduction of the sub-loading surface conveniently overcomes some limitations of the Cam-Clay models.

5. NOR-SAND

5.1 General framework

Nor-Sand **(Jefferies 1993)** is a simple elastic-plastic model for sand. It can be viewed as a sub-loading surface model, in which two surfaces exist for the two critical state conditions ($D = 0,\ \partial D/\partial \varepsilon_d^p = 0$). Unlike the Cam-Clay models, Nor-Sand is able to predict the peak state by making the state parameter to be a model variable, rather than making preconsolidation pressure p_c as a history variable in Cam-clay.

Nor-Sand was developed from Nova's stress-dilatancy flow rule **(Nova 1982)**, which is given in Eq. **50**, in the same way **Roscoe and Schofield (1963)** derived original Cam-Clay from Taylor's stress-dilatancy flow rule **(Taylor 1948).**

$$\eta' = M_\theta + (N-1)\cdot D \qquad \text{Eq. 50}$$

where N is the dilatancy parameter and M_θ the critical state stress ratio as a function of the Lode angle θ. When $N = 0$, the stress-dilatancy flow rule yields to original Cam-Clay's stress-dilatancy flow rule.

5.2 Yield surface

Nor-Sand assumes normality between the stress and the strain increments, which offers simplicity in the modelling. The integration of the stress-dilatancy rule of Eq. 50 gives two different yield functions depending on N (**Eq. 51** when $N > 0$and **Eq. 52** when $N = 0$).

$$F = \eta' - \frac{M_\theta}{N}\left[1 + (N-1)\left(\frac{p'}{p_i}\right)^{\frac{N}{1-N}}\right] \quad \text{for } N > 0 \qquad \text{Eq. 51}$$

$$F = \eta' - M_\theta\left[1 + \ln\left(\frac{p_i}{p'}\right)\right] \qquad \text{for } N = 0 \qquad \text{Eq. 52}$$

where p_i is the image pressure.

Nor-Sand sizes the yield surface with the image pressure p_i, which is an equivalent expression of the preconsolidation pressure p_c in Cam-clay. It corresponds to the pressure at the summit of the yield surface ($p'_{cs} = p_i$) rather than at the tip. The motivation in doing so is that the stress state on the yield surface is characterised by a scalar, which in turn can be used to model hardening or softening using a state parameter concept. In Cam-clay, the preconsolidation pressure p_c evolved with plastic volumetric strain. In Nor-Sand, the image pressure p_i evolves with plastic deviator strain, which is further discussed in Section 5.4.

Figure 9 shows the yield surfaces for different values of dilatancy parameter N. The summit point of the yield surface is the image condition, which is characterized by $q_i = Mp_i$. Nor-Sand is an associative flow model and hence the potential function is equal to the yield surface ($P = F$), and the strain increments are normal to the yield surface, as shown in the figure.

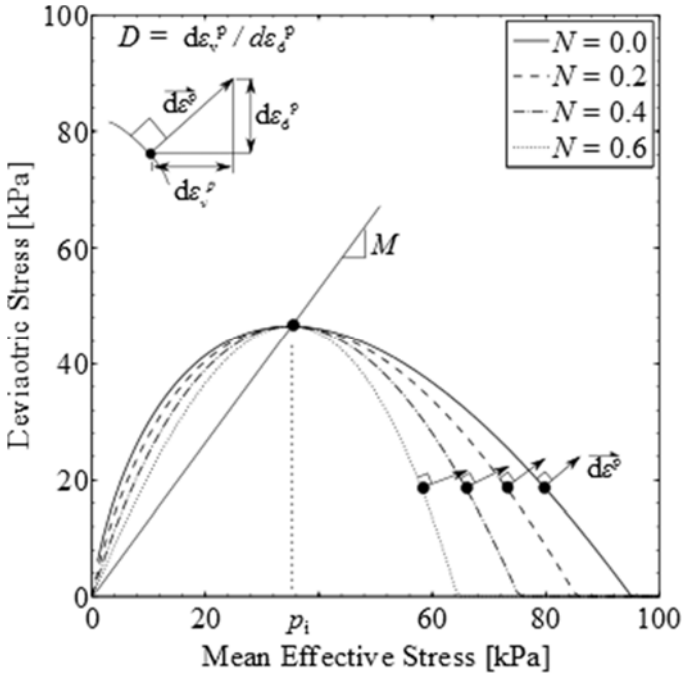

Figure 9: Yield surface of Nor-Sand

The consistency condition gives the incremental stress-strain equation of Eq. **53**.

$$d\tilde{\sigma}' = \left[\underline{D_e} - \frac{\underline{D_e} \frac{\partial F}{\partial \tilde{\sigma}'} \left(\frac{\partial F}{\partial \tilde{\sigma}'} \right)^T \underline{D_e}}{\left(\frac{\partial F}{\partial \tilde{\sigma}'} \right)^T \underline{D_e} \frac{\partial F}{\partial \tilde{\sigma}'} - \frac{\partial F}{\partial p_i} \left(\frac{\partial p_i}{\partial \tilde{\varepsilon}^p} \right)^T \frac{\partial F}{\partial \tilde{\sigma}'}} \right] d\tilde{\varepsilon} \qquad \text{Eq. 53}$$

The partial derivatives of the yield function are given by Eq. **54** to Eq. **57**.

$$\frac{\partial F}{\partial p'} = -\frac{M_\theta}{N}\left[1 + \frac{N-1}{1-N}\left(\frac{p'}{p_i}\right)^{\frac{N}{1-N}}\right] \quad \text{for } N > 0 \qquad \text{Eq. 54}$$

$$\frac{\partial F}{\partial q} = 1 \qquad \text{Eq. 55}$$

$$\frac{\partial F}{\partial M_\theta} = -\frac{p'}{N}\left[1 + (N-1)\left(\frac{p'}{p_i}\right)^{\frac{N}{1-N}}\right] \quad \text{for } N > 0 \qquad \text{Eq. 56}$$

$$\frac{\partial F}{\partial p_i} = \frac{N-1}{1-N} M_\theta \left(\frac{p'}{p_i}\right)^{\frac{1}{1-N}} \quad \text{for } N > 0 \qquad \text{Eq. 57}$$

5.3. Limit yield surface

Nor-Sand assumes that both 'wet' (loose) and 'dry' (dense) sand have an elasto-plastic hardening/softening phase, like the subloading surface model. The yield surface in Nor-Sand corresponds to the sub-loading surface in Cam-Clay. That is, the stress state of the specimen during elasto-plastic deformation is located on the yield surface. The size of the yield surface is given by p_i, instead of Rp_c in the subloading surface. However, when unloading, it behaves elastically.

Nor-Sand introduces the concept of limit yield surface with the size given by $p_{i,max}$, which is controlled by the state parameter Ψ. **Figure 10** illustrates the hardening/softening concept in Nor-Sand. When the state parameter is positive, the limit yield surface is larger than the yield surface ($p_i < p_{i,max} \rightarrow \partial p_i/\partial \varepsilon_d^p > 0$) and hardening is expected. When the state parameter is negative, the limit yield surface is smaller than the yield surface ($p_i > p_{i,max} \rightarrow \partial p_i/\partial \varepsilon_d^p < 0$) and softening is expected.

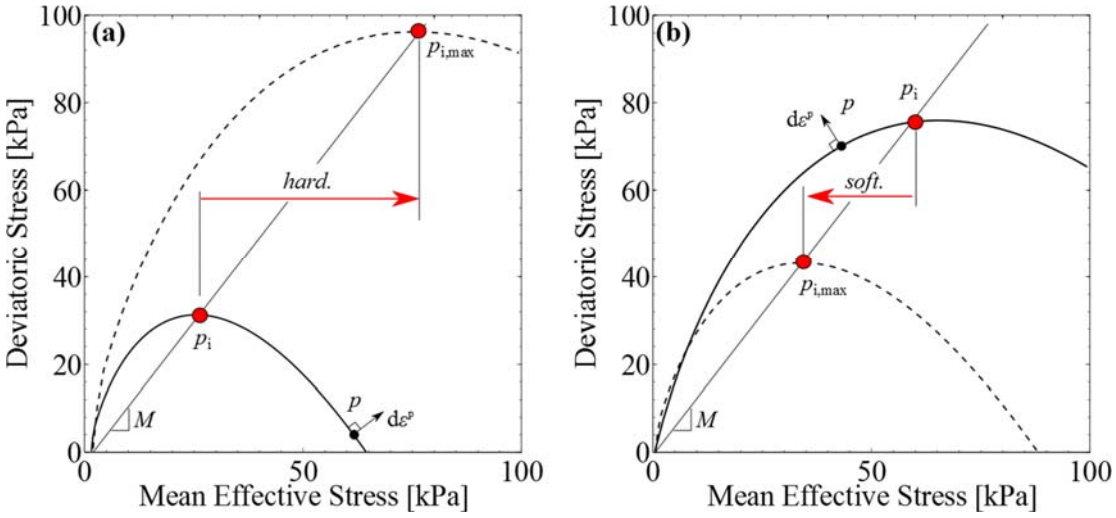

Figure 10: Hardening and softening concept in Nor-Sand

As explained in **Chapter 1**, the minimum dilatancy rate can be predicted by state indices. Nor-Sand utilizes the state parameter at image condition Ψ_i, defined in Eq. **58**.

$$\Psi_i = e - e_c(p_i) \qquad \text{Eq. 58}$$

where e is the current void ratio, and $e_c(p_i)$ is the critical state void ratio at p_i. p_i is used because hardening/softening is determined by the relative position of p_i (current yield surface) in relation to $p_{i,max}$ (limit yield surface) as shown in Figure 10.

A critical state line must be defined in order to calculate the image state parameter. As discussed in Chapter 1, **Boulanger (2003)** and **Mitchell and Soga (2005)** suggested a non-linear critical state line based on dilatancy characteristics **(Bolton 1986)**, and is expressed by **Eq. 59**.

$$e_c(p_i) = e_{max} - \frac{e_{max} - e_{min}}{\ln(Q/p_i)} \qquad \text{Eq. 59}$$

where e_{max} and e_{min} are the maximum and minimum void ratios, respectively, which are determined by laboratory tests, and Q is the crushing pressure.

The model assumes that a soil with a given Ψ_i has the minimum dilatancy rate D_{min}; that is, the soil has an ability to dilate to down to the value of D_{min}. That is, denser a soil is, more negative the dilation rate becomes at the peak stress. Jefferies and Shuttle (2011) assumed that D_{min} is proportional to Ψ_i as follows.

$$D_{min} = \chi \frac{M_\theta}{M_{tc}} \Psi_i \qquad \text{Eq. 60}$$

where χ is the model parameter, M_θ is the critical state failure angle at a given Lode angle θ and M_{tc} is the critical state failure angle at triaxial compression. It is important to note that the model is extended to both dense condition (Ψ_i<0) and loose condition (Ψ_i>0), so that it can model both hardening and softening phases.

D_{min} and $p_{i,max}$ are related to each other via the yield function. Substituting **Eq, 50** into **Eq. 51** (or **Eq. 52**), the maximum image pressure $p_{i,max}$ can be computed as Eq. **61** and Eq. **62**.

$$p_{i,max} = p \cdot \left(1 + D_{min} \frac{N}{M_{tc}}\right)^{\frac{N-1}{N}} \quad \text{for } N \neq 0 \qquad \text{Eq. 61}$$

$$p_{i,max} = p \cdot \exp\left(-\frac{D_{min}}{M_{tc}}\right) \quad \text{for } N = 0 \qquad \text{Eq. 62}$$

5.4. Hardening/softening rule

Nor-Sand assumes that the hardening/softening is governed by deviatoric plastic strains rather than volumetric plastic strains. Therefore, the following hardening/softening rule can be proposed by comparing the positions of the two surfaces or, in other words, taking the difference between $p_{i,max}$ and p_i.

$$\frac{\partial p_i}{\partial \varepsilon_d^p} = H\,(p_{i,max} - p_i) \qquad \text{Eq. 63}$$

where H is the hardening modulus.

Eq. **58** implies that p_i aims to reach to $p_{i,max}$ by shearing and the rate is controlled by H. The hardening/softening rule encapsulates the two conditions of the critical state theory. The dilatancy is nil ($D = 0$) when $p' = p_i$, and the changes in dilatancy are nil ($\partial D/\partial \varepsilon_d^p = 0$) when $p_i = p_{i,max}$. Therefore, the critical state is reached ($D = 0, \partial D/\partial \varepsilon_d^p = 0$) when $p' = p_i = p_{i,max}$.

A more complex hardening rule can be proposed to fit the experimental data. For example, **Jefferies and Shuttle (2002)** propose the following hardening/softening model.

$$\frac{\dot{p}_i}{\dot{\varepsilon}_d^p} = H \cdot \frac{M_\theta}{M_{tc}} \exp\left(1 - \frac{\eta'}{M_{tc}}\right) \cdot (p_{i,max} - p_i) \qquad \text{Eq. 64}$$

5.5 Elasticity

The current Nor-Sand model assume isotropic elastic behaviour, which requires two parameters. It is custom to assume a constant Poisson ratio ν^e and to formulate a pressure-dependent shear modulus G^e (Eq. **59**). The bulk modulus K^e can then be calculate from the shear modulus and the Poisson ratio (Eq. **65**).

$$G^e = A\left(\frac{p'}{p_{ref}}\right)^n \qquad \text{Eq. 65}$$

$$K^e = \frac{2(1+\nu^e)}{3(1-2\nu^e)} \cdot G^e \qquad \text{Eq. 66}$$

where A is the shear modulus constant, n the shear modulus exponent and p_{ref} the reference pressure.

5.7 Simulations of Drained Triaxial Compression Tests

Figure 7 (a) and (b) illustrate the simulation results of two drained triaxial compression tests, in which the specimens are consolidated isotopically to 20 kPa prior to shearing. The simulations are carried out at two different densities. Due to the low initial mean effective stress, the looser specimen ($e_0 = 0.950$) contracts at the end and the denser ($e_0 = 0.850$) dilates at the end. Therefore, these two different cases will be referred to as loose and dense specimens. The simulations were generated with a MATLAB code, which is available on the publisher's website. The model parameters and initial states are given in Table 3**.**

Table 3: Nor-Sand Model default parameters and initial conditions for simulations

A	n	ν^e	N	M_{tc}	e_{min}	e_{max}	Q	χ	H	e_0	p'_0
2500	0.5	0.2	0.3	1.33	0.542	1.00	10 MPa	3.5	200	0.950 or 0.850	20 kPa

Figure 7 (a) shows the results of the loose specimen in drained conditions ($p_i < p_{i,max}$). The results show that the specimen hardens in a non-linear way from point A to B and contracts because the stress state is on the contractive side of the yield surface ($p' > p_i$). As shearing

continues, p_i increases by the hardening rule, and at the same time $p_{i,max}$ reduces due to volume contraction. Once at point B, the mean effective stress is equal to the image pressure and the maximum image pressure ($p' = p_i = p_{i,max}$), and hence the specimen is at critical state. The dilatancy is nil and no changes in dilatancy are permitted ($D = 0,\ \partial D/\partial \varepsilon_d^p = 0$).

Figure 7 (b) shows the results of the dense specimen in drained conditions. The results show that the specimen initially contracts from point A to point B because it is on the contractive side of the yield surface ($p' > p_i$). When the stress ratio reaches the critical state stress state ($\eta' \approx M$), there is a nil dilatancy state ($p' = p_i$) because of the normality condition but still permits to harden ($D = 0,\ \partial D/\partial \varepsilon_d^p \neq 0$) because $p_i < p_{i,max}$. Therefore, the specimen is not at critical state. The shear resistance increases by p_i increasing and $p_{i,max}$ decreasing and reaches the peak state at point C. The stress ratio is maximum and the dilatancy rate becomes D_{min} with $p_i = p_{i,max}$. $p_{i,max}$ continues to decrease by dilation. The specimen starts softening from point C to point D because now $p_i > p_{i,max}$. Eventually, further shearing brings to $p' = p_i = p_{i,max}$ and the effective stress ratio and the void ratio are at critical state ($\eta' = M, e = e_{cs}$). The condition of $D = 0$ and $\partial D/\partial \varepsilon_d^p = 0$ is met and the void ratio remains the same even by continuous shearing..

5.8 Simulations of Undrained Triaxial Compression Tests

Figure 7 (c) shows the simulated behaviour of the loose specimen during undrained triaxial compression because ($p > p_i$). The specimen undergoes a short hardening phase from point A to B. The stress state is on the contractive side of the yield surface and the excess pore pressure increases. The mean effective stress decreases as the shear resistance mobilises. The peak stress state at point B in undrained conditions is significantly lower than the stress state at point B in drained conditions. The mean effective stress p' at point B is close to the critical state ($\eta' \approx M$) but not at critical state because the condition of $p_i < p_{i,max}$ still holds. As the stress ratio is slightly smaller than the critical state slope ($\eta' < M$), the specimen continues to have contractive tendency, which further increases the excess pore pressure. The reduction in mean effective stress is then accompanied by the reduction in deviator stress and hence the specimen softens from point B to point C with the condition of $p_i > p_{i,max}$. At the same time, the difference between p_i and $p_{i,max}$ reduces with increased shearing. In undrained conditions, Nor-Sand tends asymptotically towards the critical state ($p_i \rightarrow p_{i,max}$), but

mathematically it cannot reach $p_i = p_{i,max}$. Therefore, this undrained softening carries on until a nil effective stress is reached. This can be the limitation of the model.

Figure 7 (d) shows the simulated behaviour of the dense specimen during undrained triaxial compression. The stress state is initially on the contractive side ($p' > p_i$) and hence positive excess pore pressure develops from point A to B. At point B ($p' = p_i$), the dilation rate becomes zero, but it continues to increase its shear resistance because the condition of $p_i < p_{i,max}$. The stress state becomes on the dilative side of the yield surface and hence negative excess pore pressure generates. The excess pore pressure decreases and the mean effective stress increases. The deviator stress continues to rise as the difference between p_i and $p_{i,max}$ reduces with increased shearing. Again the model tends asymptotically towards the critical state $p_i \approx p_{i,max}$ but mathematically it cannot reach $p_i = p_{i,max}$. Therefore, the stress path follows slightly above the critical state line. This can be the limitation of the model.

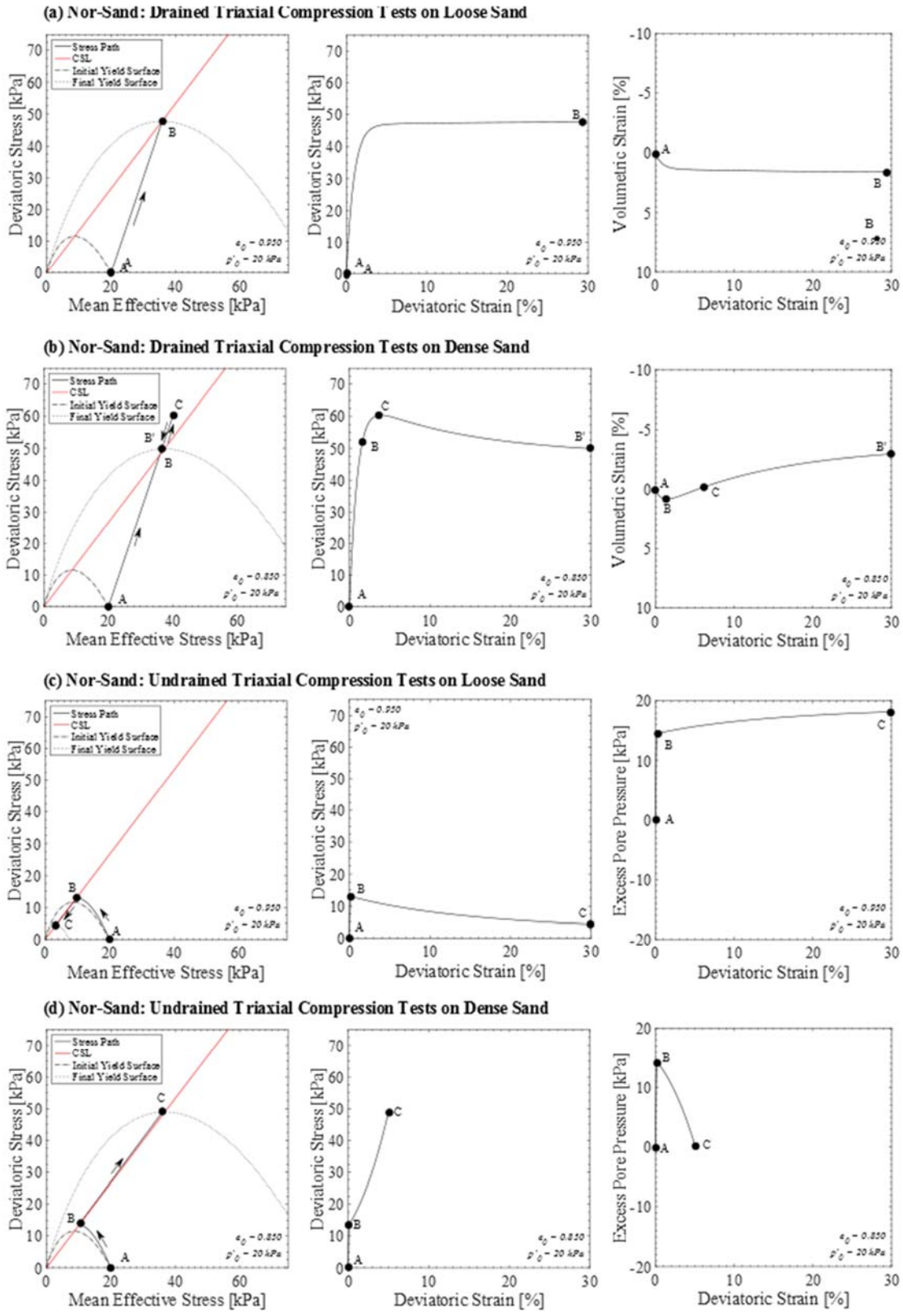

Figure 11: Triaxial compression simulations with Nor-Sand

5.9 Influence of Initial density, Dilatancy Characteristics and Hardening Moduli

Figure 12 (a) shows the effect of initial density on the stress-strain response. The peak strength, the hardening stiffness and the dilatancy rates are enhanced when the initial void ratio decreases. Mathematically, this is caused by a decrease in the image state parameter, which in turn decreases the minimum dilatancy rate D_{min} and increases the maximum image pressure, $p_{i,max}$. After reaching the peak, the specimens then soften to reach to the same critical state.

Figure 12 (b) shows the effect of dilatancy coefficient χ on the stress-strain response. An increase in χ decreases the minimum dilatancy rate D_{min} for a given image state parameter and hence gives a larger maximum image pressure $p_{i,max}$. This in turn results in enhanced peak strength and the dilatancy rate.

Figure 12 (c) shows the effect of hardening modulus H on the stress-strain response. An increase in H increases the stiffness of the soil because the rate to have $p_i = p_{i,max}$ increases. The deviator strain necessary to reach to the critical state is reduced. The volumetric change is also influenced accordingly by reducing the strain to reach D_{min}. The peak strengths are the same as the maximum image pressures $p_{i,max}$ are the same for all three tests.

5.10 Remarks on Nor-Sand

Nor-Sand was developed from the fundamental axioms of the critical state theory (Roscoe et al. 1958). Similar to the subloading surface model, it has two surfaces for each conditions ($D = 0$, $\partial D/\partial \varepsilon_d^p = 0$). These two surfaces allow a normally consolidated dense sand specimen to initially contract plastically and then dilate plastically in drained conditions, exhibiting a peak state as a consequence of this dilatancy characteristic. A normally consolidated loose sand specimen contracts plastically and hardens in drained conditions. The model can simulate the undrained case with reasonable success. Using the state parameter concept, the model can simulate rich behaviour of stress-strain relationships observed in different densities and pressures with a single set of material parameters.

Nor-Sand follows the same assumption as the critical state theory and its associated modelling framework – homogeneity, isotropy, normality, etc. Whilst it shows good abilities

in capturing the fundamental behaviour of sand and includes the density as a model variable, its original formulation, as presented in this chapter, does not include the influence of anisotropy, shear banding or even non-associative behaviour, which are common in sands. Nevertheless, it is a simple model which captures the basic mechanical behaviour of sands in an elegant manner.

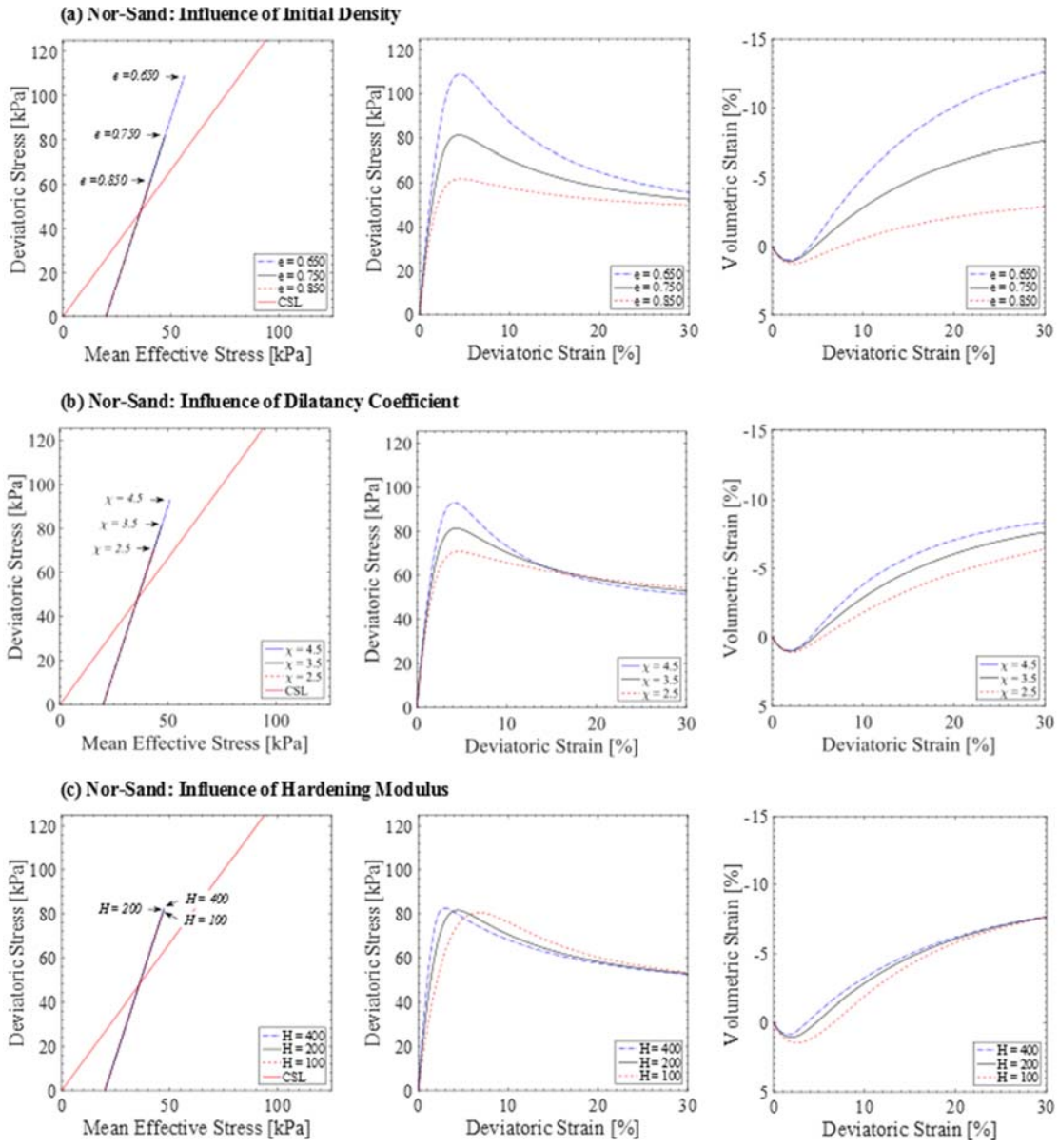

Figure 12: Sensitivity of Nor-Sand to the initial density, the dilatancy coefficient and the hardening modulus

6. CONCLUSIONS

The critical state theory presented in **Chapter 1** can be extended to develop constitutive models for granular materials. The critical state models give realistic stress-strain relationships as well as ultimate state when sheared to large strains. These models differentiate material parameters from the state parameters (such as void ratio or preconsolidation pressures). Hence, the same material parameters can be used at different depths, different densities or different stress histories as long as they are the soil of the same origin. This is why these models are powerful compared to classical Mohr-Coulomb models, in which the model parameters have to be assigned carefully depending on the state of the soil.

Cam-Clay was the first constitutive model to relate the stresses with strains based on the critical state framework. It can predict the behaviour of a wide variety of soils, from normally consolidated to overconsolidated, in both drained and undrained conditions with only 5 plastic parameters which have physical meanings and are quantifiable from element tests. However, Cam-Clay assumes that the two conditions of the critical state theory ($D = 0$, $\partial D/\partial \varepsilon_d^p = 0$) are fulfilled simultaneously and hence cannot model the peak strength as a consequence of dilatancy. The peak strength can only be modelled by sudden yielding from elastic state to plastic state.

The above limitation of Cam-Clay can be overcome by including an additional surface called the sub-loading surface. It allows decoupling of the two critical state conditions ($D = 0$, $\partial D/\partial \varepsilon_d^p = 0$). Plastic strains develop within the classical Cam-Clay yield surface and hence the peak state becomes the consequence of dilatancy. For the sub-loading surface model presented in this chapter, two additional model parameters are required and they need to be determined by fitting the model prediction to the experimental data.

Nor-Sand also decouples the two conditions of the critical state theory ($D = 0$, $\partial D/\partial \varepsilon_d^p = 0$) by introducing a limit yield surface. Nor-Sand uses the density as a model variable and can simulate the mechanical behaviour of sand rather well in both drained and undrained conditions. Like Cam-Clay models, a single set of model parameters is required to model the behaviour of a wide range of conditions.

The models presented in this chapter were developed by considering soil as an ideal homogenous continuum. Real soil consists of an aggregation of solid grains with local

variations in voids. This particulate nature can lead to local failures such as strain localisation, which may not be easily captured by the models presented here. Nevertheless, these models provide a solid foundation to simulate the development of stiffness and strength with strain and they have contributed in improving the understanding of the mechanical behaviour of clay and sand in the field of soil mechanics and geotechnical engineering.

REFERENCES

Bolton MD (1986) The strength and dilatancy of sands. Géotechnique 36:65–78.

Cole ERL (1967) The behaviour of soils in the simple shear apparatus. University of Cambridge

Coumoulos DG (1967) A radiographic study of soils. University of Cambridge

Desrues J, Chambon R, Mokni M, Mazerolle F (1996) Void ratio evolution inside shear bands in triaxial sand specimens studied by computed tomography. Géotechnique 46:529–546. doi: 10.1680/geot.1996.46.3.529

Drucker DC, Gibson RE, Henkel DJ (1957) Soil mechanics and work-hardening theories of plasticity. J Soil Mech Found Eng 122:338–346.

Hashiguchi K (1979) A Derivation of the Associated Flow Rule. J Fac Agric Kyushu Univ 24:75–80.

Hashiguchi K, Chen ZP (1998) Elastoplastic Constitutive Equation of Soils With the Subloading Surface. Int J Numer Anal Methods Geomech 22:197–227. doi: 10.1002/(SICI)1096-9853(199803)22:3<197::AID-NAG914>3.0.CO;2-T

Jefferies MG (1993) Nor-Sand : a simple critical state model for sand. Géotechnique 43:91–103.

Jefferies MG, Shuttle DA (2011) On the operating critical friction ratio in general stress states. Géotechnique 61:709–713. doi: 10.1680/geot.9.T.032

Jefferies MG, Shuttle DA (2002) Dilatancy in general Cambridge-type models. Géotechnique 52:625–638.

Mitchell JK, Soga K (2005) Fundamentals of Soil Behavior, 3rd ed. John Wiley & Sons, Hoboken

Nova R (1982) A constitutive model for soil under monotonic and cyclic loading. In: Pande GN, Zienkiewicz C (eds) Soil Mech. - transient Cycl. Load. Wiley, Chichester, pp 343–373

Roscoe KH, Burland JB (1968) On the generalised stress-strain behaviour of “wet” clay. In: Heyman J, Leckie FA (eds) Eng. Plast. Cambridge University Press, Cambridge, pp 535–609

Roscoe KH, Schofield AN (1963) Mechanical behaviour of an idealised wet clay. 2nd Eur. Conf. Soil Mech. Found. Eng. Wiesbaden, pp 47–54

Roscoe KH, Schofield AN, Wroth CP (1958) On The Yielding of Soils. Géotechnique 8:22–53. doi: 10.1680/geot.1958.8.1.22

Schofield AN, Wroth P (1968) Critical State Soil Mechanics, 2nd ed. McGraw-Hill, London

Tatsuoka F, Sakamoto M, Kawamura T, Fukushiima S (1986) Strength and deformation

characteristics of sand in plane strain compression at extremely low pressures. Soils Found 26:65–84. doi: 10.3208/sandf1972.26.65

Taylor DW (1948) Fundamentals of soil mechanics. Wiley, New York

APPENDIX A: PARTIAL DERIVATIVES

$$p' = \frac{\sigma'_1 + \sigma'_2 + \sigma'_3}{3} \quad \rightarrow \frac{\partial p'}{\partial \tilde{\sigma}'} = \begin{bmatrix} \frac{1}{3} & \frac{1}{3} & \frac{1}{3} & 0 & 0 & 0 \end{bmatrix}^T$$

$$q = \sqrt{3J_2} \quad \rightarrow \frac{\partial q}{\partial \tilde{\sigma}'} = \frac{3}{2q} \begin{bmatrix} s_1 & s_2 & s_3 & 2s_4 & 2s_5 & 2s_6 \end{bmatrix}^T$$

$$\sin 3\theta = -\frac{3\sqrt{3}}{2} \cdot \frac{J_3}{J_2^{\frac{3}{2}}} \quad \rightarrow \frac{\partial \theta}{\partial \tilde{\sigma}'} = \frac{\sqrt{3}}{2} \cdot \frac{1}{\cos 3\theta} \cdot \frac{1}{J_2^{\frac{3}{2}}} \left(\frac{\partial J_3}{\partial \tilde{\sigma}'} - \frac{3}{2} \frac{J_3}{J_2} \frac{\partial J_2}{\partial \tilde{\sigma}'} \right)$$

$$J_2 = \operatorname{tr} \tilde{s}^2 \quad \rightarrow \frac{\partial J_2}{\partial \tilde{\sigma}'} = \frac{1}{3} \begin{bmatrix} 2s_1 - s_2 - s_3 \\ -s_1 + 2s_2 - s_3 \\ -s_1 - s_2 + 2s_3 \\ 0 \\ 0 \\ 0 \end{bmatrix}$$

$$J_3 = \det \tilde{s} \quad \rightarrow \frac{\partial J_3}{\partial \tilde{\sigma}'} = \begin{bmatrix} \frac{2}{3}s_2s_3 - \frac{1}{3}s_1s_3 - \frac{1}{3}s_1s_2 + \frac{1}{3}s_4 + \frac{1}{3}s_5 - \frac{2}{3}s_6 \\ -\frac{1}{3}s_2s_3 + \frac{2}{3}s_1s_3 - \frac{1}{3}s_1s_2 + \frac{1}{3}s_4 - \frac{2}{3}s_5 + \frac{1}{3}s_6 \\ -\frac{1}{3}s_2s_3 - \frac{1}{3}s_1s_3 + \frac{2}{3}s_1s_2 - \frac{2}{3}s_4 + \frac{1}{3}s_5 + \frac{1}{3}s_6 \\ -2s_3s_4 + 2s_5s_6 \\ -2s_1s_6 + 2s_4s_5 \\ -2s_2s_5 + 2s_4s_6 \end{bmatrix}$$

$$\varepsilon_v^p = \varepsilon_1^p + \varepsilon_2^p + \varepsilon_3^p \quad \rightarrow \frac{\partial \varepsilon_v^p}{\partial \tilde{\varepsilon}^p} = \begin{bmatrix} 1 & 1 & 1 & 0 & 0 & 0 \end{bmatrix}^T$$

$$\varepsilon_d^p = \sqrt{\frac{2}{3}} \sqrt{e_1^{p\,2} + e_2^{p\,2} + e_3^{p\,2} + \frac{\gamma_4^{p\,2}}{2} + \frac{\gamma_5^{p\,2}}{2} + \frac{\gamma_6^{p\,2}}{2}}$$

$$\rightarrow \quad \frac{\partial \varepsilon_d^p}{\partial \tilde{\varepsilon}^p} = \frac{1}{3\varepsilon_d^p} \begin{bmatrix} \frac{4}{3}e_1^p - \frac{2}{3}e_2^p - \frac{2}{3}e_3^p \\ -\frac{2}{3}e_1^p + \frac{4}{3}e_2^p - \frac{2}{3}e_3^p \\ -\frac{2}{3}e_1^p - \frac{2}{3}e_2^p + \frac{4}{3}e_3^p \\ \gamma_4^p \\ \gamma_5^p \\ \gamma_6^p \end{bmatrix}$$